Received: 21 April 2020 | Revised: 4 August 2020 | Accepted: 14 August 2020

DOI: 10.1111/cas.14620

ORIGINAL ARTICLE

Cancer Science WILEY

Deficiency of pseudogene UPAT leads to hepatocellular carcinoma progression and forms a positive feedback loop with ZEB1

Leyang Xiang[1,2] | Xiaoting Huang[3] | Siqi Wang[4] | Huohui Ou[5] | Zhanjun Chen[1,6] | Zhigang Hu[1] | Yu Huang[7] | Xianghong Li[1] | Yawei Yuan[3] | Dinghua Yang[1]

[1]Unit of Hepatobiliary Surgery, Department of General Surgery, Nanfang Hospital, Southern Medical University, Guangzhou, China

[2]Department of Oncology Surgery, Affiliated Cancer Hospital & Institute of Guangzhou Medical University, Guangzhou, China

[3]Department of Radiation Oncology, Affiliated Cancer Hospital & Institute of Guangzhou Medical University, Guangzhou, China

[4]Department of gastroenterology, Nanfang Hospital, Southern Medical University, Guangzhou, China

[5]Department of Hepatobiliary Surgery, Shunde Hospital, Southern Medical University (The First People's Hospital of Shunde), Foshan, China

[6]Department of General Surgery, Affiliated Baoan Hospital of Shenzhen, Southern Medical University, Shenzhen, China

[7]Department of Laboratory Medicine, Nanfang Hospital, Southern Medical University, Guangzhou, China

Correspondence
Dinghua Yang, Unit of Hepatobiliary Surgery, Department of General Surgery, Nanfang Hospital, Southern Medical University, 1838 North Guangzhou Avenue, Baiyun District, Guangzhou 510515, China.
Emails: dhyangyd@yahoo.com; nfyangdh@163.com

Yawei Yuan, Department of Radiation Oncology, Affiliated Cancer Hospital & Institute of Guangzhou Medical University, Guangzhou, Guangdong Province 510095, China.
Email: yuanyawei2015@outlook.com

Funding information
Guangdong Provincial Science and Technology Projects, Grant/Award Number: 2017A020215132; National Natural Science Foundation of China, Grant/Award Number: 81872385

Abstract

Hepatocellular carcinoma (HCC) is a common disease worldwide. Accumulating reports have evidenced the internal connection between epithelial-mesenchymal transition (EMT) and cancer stem cells (CSCs), as well as their significance in metastasis and post–operative recurrence. In this study, we investigated an interesting ubiquitin-proteasome pathway associated pseudogene of AOC4, also known as UPAT, and showed that it was downregulated in 39.78% (37/93) of patients with hepatitis B virus (HBV)-related HCC. Downregulation of UPAT was associated with multiple worse clinicopathological parameters, as well as decreased recurrence-free survival (RFS). In vitro and in vivo assays found that overexpression of UPAT significantly suppressed cellular migration, invasion, EMT processes, and CSC properties. Mechanistic studies showed that UPAT promoted ZEB1 degradation via a ubiquitin-proteasome pathway and, in contrast, ZEB1 transcriptionally suppressed UPAT by binding to multiple E-box (CACCTG) elements in the promoter region. Moreover, UPAT was negatively correlated with ZEB1 protein in HCC tissues, their combined expression discriminated RFS outcomes for patients with HBV-related HCC. These

Abbreviations: AFP, alpha-fetoprotein; AOC4, amine oxidase, copper containing 4; ChIP, chromatin immunoprecipitation; Co-IP, co-immunoprecipitation; CSCs, cancer stem cells; EMT, epithelial-mesenchymal transition; GO, gene ontology; HBV, hepatitis B virus; HCC, hepatocellular carcinoma; HCV, hepatitis C virus; IF, immunofluorescence; IHC, immunohistochemical; RFS, recurrence-free survival; RIP, RNA immunoprecipitation; RT-qPCR, real-time quantitative PCR; siRNA, small interfering RNA; TF, transcriptional factors; UHRF1, Ubiquitin-like plant Homeodomain (PHD) and Really interesting new gene (RING) Finger domain containing protein 1; UPAT, UHRF1 Protein Associated Transcript; WB, western blotting.

Leyang Xiang and Xiaoting Huang contributed equally to this work.

data on the UPAT-ZEB1 circuit-mediated pathway will further knowledge on EMT and CSCs, and may help to develop novel therapeutic approaches for the prevention of HCC metastasis.

KEYWORDS

epithelial-mesenchymal transition, hepatocellular carcinoma, stemness, UPAT, ZEB1

1 | INTRODUCTION

Hepatocellular carcinoma (HCC), the most frequent primary liver cancer, is ranked as the sixth most common disease and fourth leading cause of cancer-associated death worldwide.[1,2] Hepatitis B virus (HBV) and hepatitis C virus (HCV) are the most frequent risk factors for HCC, their contribution to HCC incidence varies between different regions due to the varied prevalence of HBV or HCV in the population.[3] In GLOBOCAN 2018 estimates of cancer incidence, approximately half the total number of HCC patients occurred in mainland China[2] and at least 85%-90% of them were HBV-related HCC.[4] Although surgical resection, liver transplantation, and ablation are radical treatments for early-staging patients, metastatic recurrence always complicates the post–operative prognosis in 70% of patients with disease at 5 years[5]. Moreover, the majority of treatment-naïve HCC patients are diagnosed with intra- or extra-hepatic metastasis.[1] Therefore, illuminating the molecular mechanisms that control HCC metastasis, particularly in HBV infection characteristics, is urgent, and crucial.

EMT is a well understood process in which epithelial cancer cells acquire migratory and invasive abilities and leave primary locations to form metastatic lesions.[6] Signaling pathways, such as TGF-β, VEGF, IGF, Wnt, and Notch, and EMT-associated transcriptional factors (EMT-TFs), such as Snail, Slug, ZEB1/2, TWIST, and others, are critical inducers and regulators of EMT.[7,8] At this time, EMT progression is known as a crucial regulator of the cancer stem cell (CSC) phenotype, and helps to induce the cellular and functional heterogeneity inherent with its self-renewal and differentiation properties, as well as generate metastatic CSCs, and subsequently results in tumor dissemination, recurrence, and metastasis.[8-10] Mechanistic studies have also proposed that activation of EMT induces autocrine signaling loops (TGF-β/SMAD and Wnt/β-catenin pathways), which are responsible for the acquisition of stemness of non-CSC cancer cells.[11] Moreover, EMT-TFs were observed to be significantly enriched in CSCs, both in murine and human breast cancers.[12] Therefore, elucidating the EMT-CSC-associated regulatory networks undoubtedly will contribute to the deeper understanding of HCC metastasis.

UPAT (ubiquitin-like plant Homeodomain (PHD) and RING finger domain containing protein 1 [UHRF1] Protein Associated Transcript), a pseudogene of amine oxidase, copper containing 4 (AOC4), is also known as a long noncoding RNA (lncRNA) of 2073 nt at length. In humans, a single base change at position 225 of AOC4 converts a codon for tryptophan to a stop codon, which results in a truncated, non-functional protein; this truncated protein is believed to be derived from proteolytic release of vascular adhesion protein 1 (VAP-1) encoded by AOC3.[13] Interestingly, AOC4 mRNA, namely AOC4P or UPAT here, is known to regulating tumorigenesis and cancer progression, and its expression and function varies with cancer types. Taniue et al[14] first reported the oncogenic effect of UPAT in colon tumorigenesis by inhibiting TrCP-mediated UHRF1 degradation but, unfortunately, UPAT expression was not evaluated in colon cancer tissues. In gastric cancer and gastrointestinal stromal tumors, UPAT was thought to be upregulated in tumor tissues and positively correlated with greater proliferative, migrative, and invasive abilities, as well as the transition from epithelial to mesenchymal states.[15,16] Another study, however, reported that UPAT was significantly downregulated in HCC and negatively correlated with worse clinicopathological parameters. It inhibits migration and invasion by suppressing the EMT process, during which expression of 2 EMT-associated TFs, Snail1 and Twist was reduced. Moreover, UPAT interacted with vimentin and accelerated its degradation. These results indicated the suppressive effect of UPAT on HCC progression.[17] However, UPAT-induced vimentin degradation, as an effective process of EMT, was not enough to enhance the promotion of EMT, or the conversion from non-CSCs to CSCs. Considering the divergent roles of UPAT in cancers, some essential mechanisms not illuminated previously must exist.

ZEB1 is aberrantly expressed in a variety of human cancers (including HCC) as one of the well defined EMT drivers, as it controls the stemness of cancer cells by multiple pathways.[18] It transcriptionally represses the expression of the miR-200 family, which together control the expression of CSC-related TFs, such as SOX2, KLF4, and BMI1.[19,20] ZEB1 also dramatically promotes the transition of basal breast cancer from non-CSC populations to CSCs in response to microenvironmental signals, such as TGF-β.[21] Additionally, ZEB1 controls CD44 variants splicing by suppression of ESRP1 in breast and pancreatic cancers. In contrast, CD44 variants activate the expression of ZEB1 and, by this self-enforcing CD44s/ZEB1 feedback loop, cancer cells maintain EMT and CSCs traits.[22] These studies together placed ZEB1 as a central regulator in orchestrating the stemness and EMT in cancers.

In this study, we determined UPAT expression in a cohort of HBV-related HCC patients, the effect of UPAT on EMT and CSCs trait was systematically explored, followed by the mechanistic study on the interplay of UPAT with the important EMT-related and CSC-related TF, ZEB1.

2 | MATERIALS AND METHODS

2.1 | Patients and specimens

In total, 93 paired HCC and adjacent noncancerous liver tissues from patients who were initially diagnosed with HBV-related HCC and received radical resection between November 2010 and July 2015 in Nanfang Hospital, Southern Medical University were collected. The Ethical Committee of Nanfang Hospital, Southern Medical University approved this research. As required by the World Medical Association Declaration of Helsinki, written consent was signed by each patient. All patients received regular follow-up and standard anti-HBV therapy to inhibit viral replication or reactivation using nucleotide drugs. The follow-up began at the date of surgery, and terminated on April 30, 2019. Five patients were lost to follow-up, 2 were removed from prognostic analysis because of post–operative complication-related death.

2.2 | Cell lines and culture conditions

MHCCLM3, MHCC97H, and MHCC97L were obtained from Liver Cancer Research Institute, Zhongshan Hospital, Fudan University, Shanghai, China. SNU-449, SNU-387, SK-hep1, and HepG2 were purchased from the American Type Culture Collection (ATCC; VA, USA). BEL-7402, SMMC-7721, Huh7, and a human immortalized liver cell line LO2 were bought from the Institutes of Biological Sciences, Chinese Academy of Sciences, Shanghai, China. MHCCLM3, MHCC97H, MHCC97L, Huh7, HepG2, and SK-hep1 were maintained in DMEM medium (Gibco), while others were grown in RPMI-1640 medium (Gibco) at 37°C in a humidified atmosphere with 5% CO_2 in air. Both basic media were supplemented with 10% fetal bovine serum (Gibco).

2.3 | Real-time quantitative PCR (RT-qPCR)

Total RNA was isolated from cell lines and liquid nitrogen-stored human tissues using RNAiso Plus reagent (Takara), and 1 μg RNA was then reverse transcribed to cDNA using a PrimeScript first-strand cDNA synthesis kit in accordance with the manufacturer's instructions (TaKaRa). The RT-qPCR primers for UPAT, ZEB1, and 18S rRNA are listed in Table S1. RT-qPCR detection was performed using a SYBR Premix Ex Taq™ kit (TaKaRa) on a LightCycler 480 II System (Roche) in accordance with the manufacturer′s instructions. The $2^{-\Delta\Delta C_T}$ method was used to analyze the relative expression of target genes by normalization to 18S rRNA.

2.4 | Subcellular fractionation and RNA quantification

A cytoplasmic and nuclear extraction kit (BestBio) was used to separate the cytoplasmic and nuclear fractions of HCC cells in accordance with the manufacturer's instructions; cytoplasmic and nuclear RNAs were respectively isolated using a HiPure total RNA nano kit (Magen). GAPDH (primary located at the cytoplasm) and U1 snRNP (primary located at the nucleus) were used as positive controls. The expression levels of UPAT, U1 snRNP, and GAPDH in the cytoplasm and nucleus were evaluated by RT-qPCR and normalized to β-actin mRNA. All experiments were repeated 3 times, and the primers are listed in Table S1.

2.5 | Transfection with lentivirus, small interfering RNA (siRNA), and plasmids

For UPAT overexpression, human UPAT transcript was synthesized and cloned into GV358 (Ubi-MCS-3FLAG-SV40-EGFP-IRES-puromycin) by Genechem (Shanghai, China). BEL-7402 and Huh7 were transfected with UPAT-overexpression lentivirus (Lv-UPAT group) or empty GV358 (Vector group) at a multiplicity of infection (MOI) of 50, and SNU-449 at a MOI of 20. Cells expressing green fluorescent protein (GFP), indicating the successfully transfection, were observed visually under an inverted fluorescence microscope (Olympus) and fluorescence-activated cell sorting (FACS) system.

For ZEB1 transient knockdown, siRNA (sense strand, 5′-GTCTGGGTGTAATCGTAAATTC) targeting ZEB1 was designed and synthesized by RiboBio Co., Ltd. The siRNA was transfected into SNU-449 cells using lipofectamine 3000 reagent (Invitrogen), after 48 h cells were collected for further analyses.

Plasmid (Ubi-MCS-3FLAG-SV40-EGFR-IRES-puromycin) containing ZEB1 cDNA (NM_00112828) or vector were bought from Genechem Co., Ltd. Equal amounts of ZEB1-overexpression or vector plasmids were transfected into SNU-449 cells using lipofectamine 3000 reagent (Invitrogen). At 48 h later, the transfected cells were subjected to further assays.

2.6 | Cell proliferation assays

Cell proliferation was evaluated by CCK-8 and plate colony-forming assays 3 times, respectively. For the CCK-8 assay, approximately 2000 cells were seeded into 96-well plates. After adhesion and 0, 24, 48, 72, or 96 h of culture, the absorbance at 450 nm was detected using CCK-8 reagent (Dojindo Laboratories) on a microplate reader (SpectraMax Plus 384; Molecular Devices). For the plate colony-forming assay, 400 cells were seeded onto 6-well plates and maintained for 2 wk. Then, 4% paraformaldehyde-fixed and 0.5% crystal violet-stained colonies were imaged using the FluorChem E system (ProteinSimple) and manually counted.

2.7 | Transwell assays

Cellular migrative and invasive abilities were assessed by Transwell assay 3 times. In brief, 5×10^4 liver cancer cells were suspended in

200 μL FBS-free medium and seeded in upper chambers (Corning) inserted into 24-well plates, and 500 μL complete medium was added to the lower chambers. For the invasion assay, the membranes of the chambers were coated with Matrigel (Corning), which was diluted with FBS-free medium at a ratio of 1:8. After 12 (SNU-449) or 24 h (BEL-7402, Huh7) incubation, cells that penetrated the filters were fixed with 4% paraformaldehyde, stained with 0.5% crystal violet, and photographed under a microscope (Olympus).

2.8 | Western blotting

Cells were lysed with RIPA lysis buffer (Beyotime) containing 1 mM protease inhibitor PMSF. After centrifugation at 12 000 *g* for 30 min at 4°C, the supernatants were collected for further protein concentration determination using the bicinchoninic acid (BCA) method (Beyotime). Then, the denatured proteins were separated with 10% SDS-PAGE electrophoresis and transferred onto PVDF membranes (Millipore). The membranes were blocked with TBST solution supplemented with 5% skimmed milk for 1 h at room temperature, incubated with primary antibodies (Table S2) overnight at 4°C and then with secondary antibodies (Table S2) for 1 h at room temperature. Finally, the protein bands were visualized using a ECL substrate kit (Fdbio Science) and the FluorChem E system (ProteinSimple).

2.9 | Immunohistochemical (IHC) staining

Immunohistochemical staining and scoring method were performed as previously reported. ZEB1 protein expression in the nucleus was evaluated semiquantitatively by multiplying staining intensity and positive cell percentage scored under an upright microscope (Olympus), while the staining intensity was scored as follows: 0, negative, 1, weak, 2, moderate, and 3, strong. The percentage of positive cells was judged as follows: 1, 1%-25% positive cells, 2, 26%-49% positive cells, 3, 50%-75% positive cells, 4, >75% positive cells.[23] A score ≥1 was regarded as positive expression of ZEB1. The antibodies are list in Table S2.

2.10 | Immunofluorescence (IF) staining

HCC cells seeded on coverslips were 4% paraformaldehyde-fixed for 20 min, permeabilized with 0.3% Triton X-100 at room temperature (40 min for nuclear proteins, 20 min for cytosolic proteins or without this procedure for membrane proteins). Then, slides were blocked with 3% BSA for 1 h at room temperature, followed by incubation with primary antibodies (Table S2) overnight at 4°C. The next day, all the followed procedures were performed in the dark at room temperature. The slides were incubated with Alexa fluor 594-conjugated goat-anti-rabbit secondary antibody (Proteintech) for 1 h, and the nucleus was stained with DAPI (Solarbio) for 10 min. Images were captured using an inverted fluorescence microscope (Olympus). The fluorescence intensity was evaluated using ImageJ software (NIH, USA).

2.11 | Spheroid colony formation assay

Spheroid colony formation assay was performed using Lv-UPAT and empty vectors transfected Huh7 cells 3 times. Lv-UPAT and vector Huh7 cells in logarithmic growth phase were resuspended in BSA-free DMEM/F12 medium (Gibco), then approximately 500 cells in each group were seeded into a non-adherent 6-well plates (Corning) and maintained in DMEM/F12 medium containing 10 μL/mL B27 (Gibco), 10 ng/mL bFGF (Gibco), and 20 ng/mL EGF (Gibco) for 2 wk. The non-adherent spheroid clusters were collected by low speed centrifugation (400 rpm), observed, and manually counted under an inverted fluorescence microscope (Olympus).

2.12 | Tumorigenicity assay

Male BALB/c nude mice (4-5 wk old) were purchased from the Central Laboratory of Animal Science, Southern Medical University (Guangzhou, China) and kept in specific pathogen-free conditions. Animal experiments were approved by the Institutional Animal Care and Use Committee of Southern Medical University, and performed in accordance with the Guide for the Care and Use of Laboratory Animals.

In total, 1×10^7 SNU-449 cells with stably overexpressing UPAT or empty vector were subcutaneously injected into the left flank regions of each mouse. The tumor growth was evaluated every 4 d by measuring the length and width. The tumor volume was calculated with the following formula: $V = \text{length} \times \text{width} \times \text{width} \times \frac{\pi}{6}$. After 28 d, the mice were sacrificed, and the samples were collected and fixed in paraformaldehyde for IHC staining.

2.13 | RNA immunoprecipitation (RIP)

RIP assay was performed to confirm the binding of ZEB1 with UPAT using an RNA Binding Protein Immunoprecipitation Kit (BersinBio) in accordance with the manufacturer's instructions. In brief, SNU-449 cells grown in a 15 cm plate were collected and lysed in RNA lysis buffer supplemented with protease and RNase inhibitors. The lysates were immunoprecipitated separately with anti-ZEB1 rabbit antibody (Cell Signaling Technology) and control IgG at 4°C overnight with gentle rotation and then incubated with protein A/G magnetic beads at 4°C for 1 h. Then, the co-precipitated RNAs were extracted using a HiPure total RNA nano kit (Magen), the level of UPAT was quantitated with RT-qPCR. All experiments were repeated 3 times.

2.14 | Prediction of TFs

The promotor region of UPAT (upstream 2000 bases to downstream 200 bp of UPAT in the genome) was obtained from the University

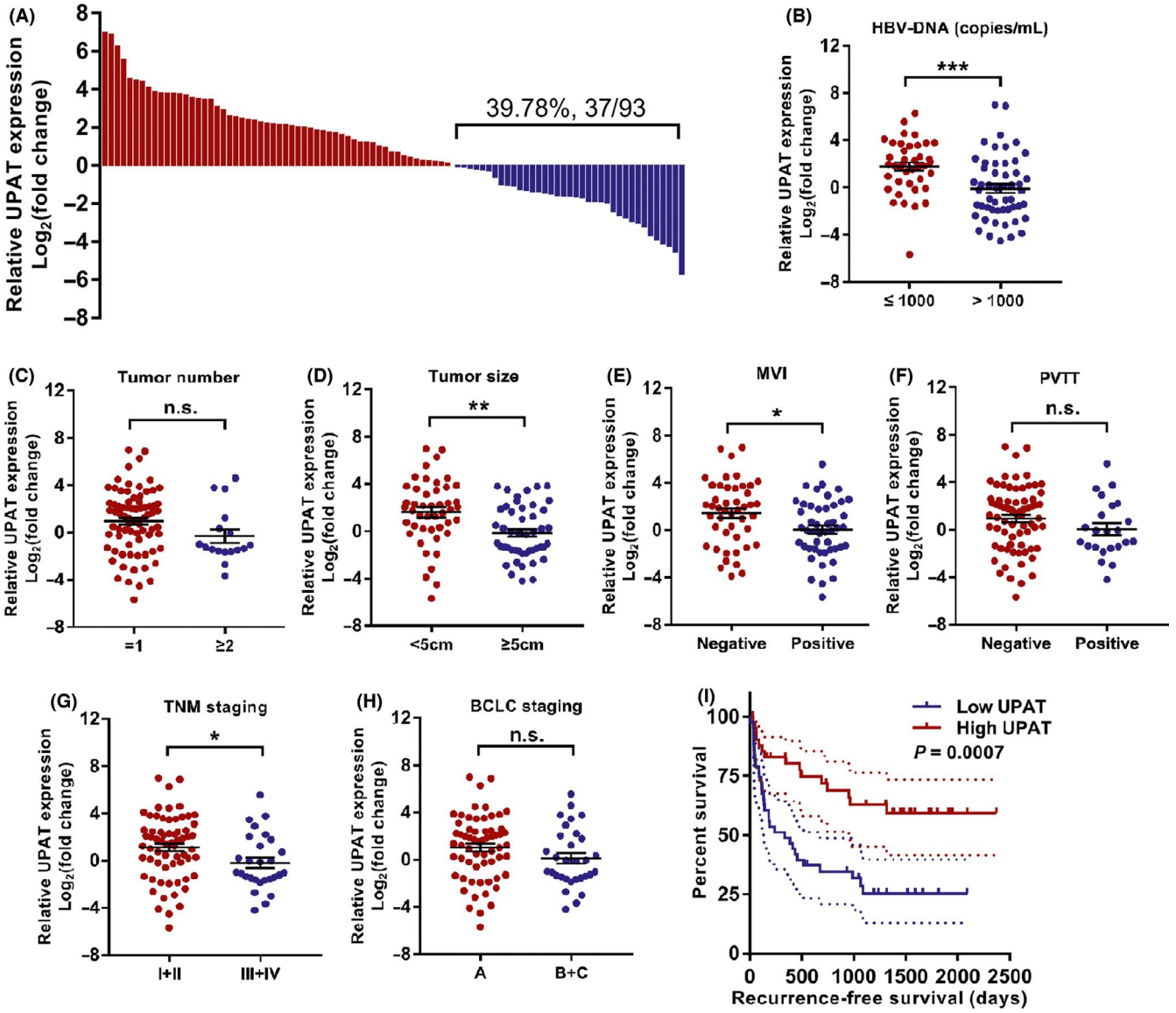

FIGURE 1 UHRF1 Protein Associated Transcript (UPAT) expression in patients with hepatitis B virus (HBV)-related hepatocellular carcinoma (HCC) and its clinical significance. A, Relative UPAT expression in patients with HBV-related HCC determined by RT-qPCR, results were presented after logarithmic transformation (n = 93). B-H, Comparison of relative UPAT expression in patients grouped HBV-DNA copies (B), tumor number (C), tumor size (D), microvascular invasion (MVI) status (E), portal vein tumor thrombosis (PVTT) (F), TNM (G), and Barcelona clinic liver cancer (BCLC) staging (H) evaluated by unpaired *t* test. I, Comparison of recurrence-free survival (RFS) using Kaplan-Meier method and log-rank *t* test in HCC patients grouped with relative UPAT expression. n.s., not significant; $^{*}P < .05$; $^{**}P < .01$; $^{***}P < .001$

of California, Santa Cruz (UCSC),[24] the TFs targeting the promotor region of UPAT were predicted using JASPAR.[25]

2.15 | Co-immunoprecipitation (Co-IP)

The Co-IP experiment was performed to enrich ZEB1 protein in Lv-UPAT and vector SNU-449 cells with or without MG-132 treatment. Cell lysates were supplemented with proteinase inhibitor cocktail (MCE) and incubated with anti-ZEB1 rabbit monoclonal antibody (#70512; 1:50; Cell Signaling Technology) overnight at 4°C. Then, the cell lysate-antibody mix was incubated with BSA blocked protein G Dynabeads (Invitrogen) for 2 h at 4°C. After washing with ice-cold PBS buffer 3 times, the complexes were eluted with loading buffer and denatured for 10 min at 100°C. Finally, the complexes containing enriched ZEB1 protein were subjected to ZEB1 ubiquitination detection by WB.

2.16 | Chromatin immunoprecipitation (CHIP)

To verify the direct binding of ZEB1 to the UPAT promoter region, CHIP assay was performed on SNU-449 cell using the reagents provided by the SimpleChIP® Enzymatic Chromatin IP Kit (CST9002; Cell

TABLE 1 Correlation between relative UPAT expression and clinicopathological characteristics of hepatocellular carcinoma (n = 93)

Clinicopathological parameter	UPAT expression[a]		χ^2	*P*-value
	Low (n = 47)	High (n = 46)		
Gender				
Male	39 (49.4%)	40 (50.6%)	0.288	.592
Female	8 (57.1%)	6 (42.9%)		
Age				
<60	40 (51.9%)	37 (48.1%)	0.356	.551
≥60	7 (43.8%)	9 (56.2%)		
HBV-DNA (copies/mL)				
<1000	12 (29.3%)	29 (70.7%)	13.270	.000
≥1000	35 (67.3%)	17 (32.7%)		
AFP (μg/L)				
<400	28 (51.9%)	26 (48.1%)	0.089	.765
≥400	19 (48.7%)	20 (51.3%)		
Cirrhosis				
Negative	12 (54.5%)	10 (45.5%)	0.185	.667
Positive	35 (49.3%)	36 (50.7%)		
Tumor number				
1	34 (44.7%)	42 (55.3%)	5.597	.018
≥2	13 (76.5%)	4 (23.5%)		
Tumor size (cm)				
<5.0	16 (34.8%)	30 (65.2%)	9.038	.003
≥5.0	31 (66.0%)	16 (34.0%)		
Tumor capsule				
Negative	13 (59.1%)	9 (40.9%)	0.843	.358
Positive	34 (47.9%)	37 (52.1%)		
Differentiation				
Poor	15 (68.2%)	7 (31.8%)	5.916	.052
Moderate	29 (49.2%)	30 (50.8%)		
Well	3 (25.0%)	9 (75.0%)		
MVI				
Negative	16 (34.8%)	30 (65.2%)	9.038	.003
Positive	31 (66.0%)	16 (34.0%)		
PVTT				
Negative	31 (44.3%)	39 (55.7%)	4.426	.035
Positive	16 (69.6%)	7 (30.4%)		
TNM stage				
I + II	27 (41.5%)	38 (58.5%)	6.994	.008
III + VI	20 (71.4%)	8 (28.6%)		
BCLC stage				
A	26 (41.9%)	36 (58.1%)	5.506	.019
B + C	21 (67.7%)	10 (32.3%)		

Abbreviations: AFP, alpha-fetoprotein; BCLC, Barcelona clinic liver cancer; MVI, microvascular invasion; PVTT, portal vein tumor thrombosis; TNM, tumor–node–metastasis.

[a]Patients with HCC were divided into low (≤ median)/high (> median) UPAT expression groups using the median as cutoff value, median = 1.641.

TABLE 2 Univariate and multivariate Cox regression analyses for RFS of patients with HCC (n = 86)[a]

Clinicopathological parameter	HR	95% CI	*P*-value
Univariate analysis			
Age (<60 vs ≥60 y)	1.084	0.509-2.309	.834
Gender (male vs female)	0.475	0.171-1.319	.153
HBV copies (<1000 vs ≥1000)	1.638	0.928-2.892	.089
AFP (<400 vs ≥400)	1.200	0.687-2.097	.521
Liver cirrhosis (positive vs negative)	1.214	0.608-2.424	.583
Capsule (positive vs negative)	1.309	0.671-2.553	.430
Tumor size (<5.0 vs ≥ 5.0 cm)	2.846	1.570-5.160	.001
Tumor number (1 vs ≥2)	2.696	1.404-5.179	.003
MVI (positive vs negative)	4.162	2.262-7.659	.000
PVTT (positive vs negative)	3.384	1.863-6.145	.000
Differentiation (well, moderate, poor)	0.399	0.247-0.644	.000
UPAT (high vs low)	0.352	0.189-0.655	.001
Multivariate analysis			
Tumor size (<5.0 vs ≥5.0 cm)	1.437	0.693-2.981	.330
Tumor number (1 vs ≥2)	3.010	1.402-6.463	.005
MVI (positive vs negative)	3.706	1.635-8.398	.002
PVTT (positive vs negative)	0.994	0.470-2.104	.988
Differentiation (well, moderate, poor)	0.683	0.394-1.183	.174
UPAT (high vs low)	0.687	0.345-1.369	.286

Abbreviations: AFP, alpha-fetoprotein; CI, confidence interval; HBV, hepatitis B virus; MVI, microvascular invasion; PVTT, portal vein tumor thrombosis.

[a]Five patients were loss to follow-up, 2 were removed from prognostic analysis because of post–operative complication-related death.

Signaling Technology) as per the manufacturer's instructions. Rabbit polyclonal antibodies against ZEB1 (Cell Signaling Technology) and rabbit IgG were employed. The eluted DNA was subjected to subsequent PCR analysis using a PCR Purification Kit (Qiagen). The primers used are shown in Table S1.

2.17 | Dual-luciferase reporter assay

SNU-449 cells were seeded into a 24-well plate and grown until 70% confluency and then co-transfected with ZEB1 overexpression (NM_00112828) or vector plasmids and pGL3-basic luciferase reporter plasmids (Kidan Biosciences) that contained either the whole predicated promoter of UPAT (pGL3-UPAT wild-type; pGL3-UPAT-WT) or binding site 1-deleted promoter region (pGL3-Del-site 1) using lipofectamine 3000 (Invitrogen). After 48 h, firefly and Renilla luciferase activities were measured using the dual-luciferase reporter system (Promega) with a luminometer (TD-20/20; EG&G Berthold), and firefly luciferase enzyme activity was normalized to Renilla luciferase enzyme activity. The dual-luciferase reporter assay was repeated independently 3 times.

2.18 | Statistics

Statistical analyses were performed using SPSS Statistics 20.0 software (SPSS, Inc), and results are shown as mean ± standard error of mean (SEM). The counting data were analyzed by chi-square test. Measurement data were compared by Student *t* test, Mann-Whitney *U* test, and analysis of variance (ANOVA) followed by least significant difference (LSD) *t* test or Dunnett's T3 test as appropriate. Survival between groups was assessed by the Kaplan-Meier method and log-rank test. The correlation coefficient between 2 groups was evaluated by Pearson correlation analysis. A *P*-value < .05 was considered as statistically significant.

3 | RESULTS

3.1 | Downregulation of UPAT predicates poor prognosis of HBV-related HCC

To research the potential effect of pseudogene UPAT in HCC, we first determined its relative expression by RT-qPCR using cancerous and adjacent noncancerous liver tissues. As shown in Figure 1A, relative UPAT expression was downregulated in 39.78% (37/93) of patients with HBV-related HCC, and those with detectable HBV-DNA in venous blood ($P < .001$), multiple tumor lesions ($P = .018$), tumor size ≥5 cm ($P = 0.003$), microvascular invasion (MVI; $P = 0.003$), portal vein tumor thrombosis (PVTT; $P = 0.035$), progressive TNM ($P = 0.008$) and Barcelona clinic liver cancer (BCLC) ($P = .019$) staging, were inclined to have lower relative UPAT expression, as revealed by chi-square test (Table 1). Furthermore, similar results were also obtained using *t* test (Figure 1B-H). Moreover, patients with lower relative UPAT expression had shorter RFS times compared with those with higher relative UPAT expression (median, 336 d vs undefined; $P = 0.0007$; Figure 1I). Univariate Cox regression analyses indicated that tumor size (95% confidence interval [CI], 1.570-5.160, $P = .001$), tumor number (95% CI, 1.404-5.179; $P = .003$), MVI (95% CI, 2.262-7.659; $P < .001$), PVTT (95% CI, 1.863-6.145, $P < .001$), differentiation (95% CI, 0.247-0.644; $P < .001$), and relative UPAT expression (95% CI, 0.189-0.655; $P = .001$) were prognostic factors for RFS in patients with HCC. Of them, tumor number (95% CI, 1.402-6.463; $P = 0.005$) and MVI (95% CI, 0.470-2.104; $P = 0.002$) were independent risk factors for RFS (Table 2). These results indicated that downregulation of UPAT in HCC tissues was a risk factor for HCC progression.

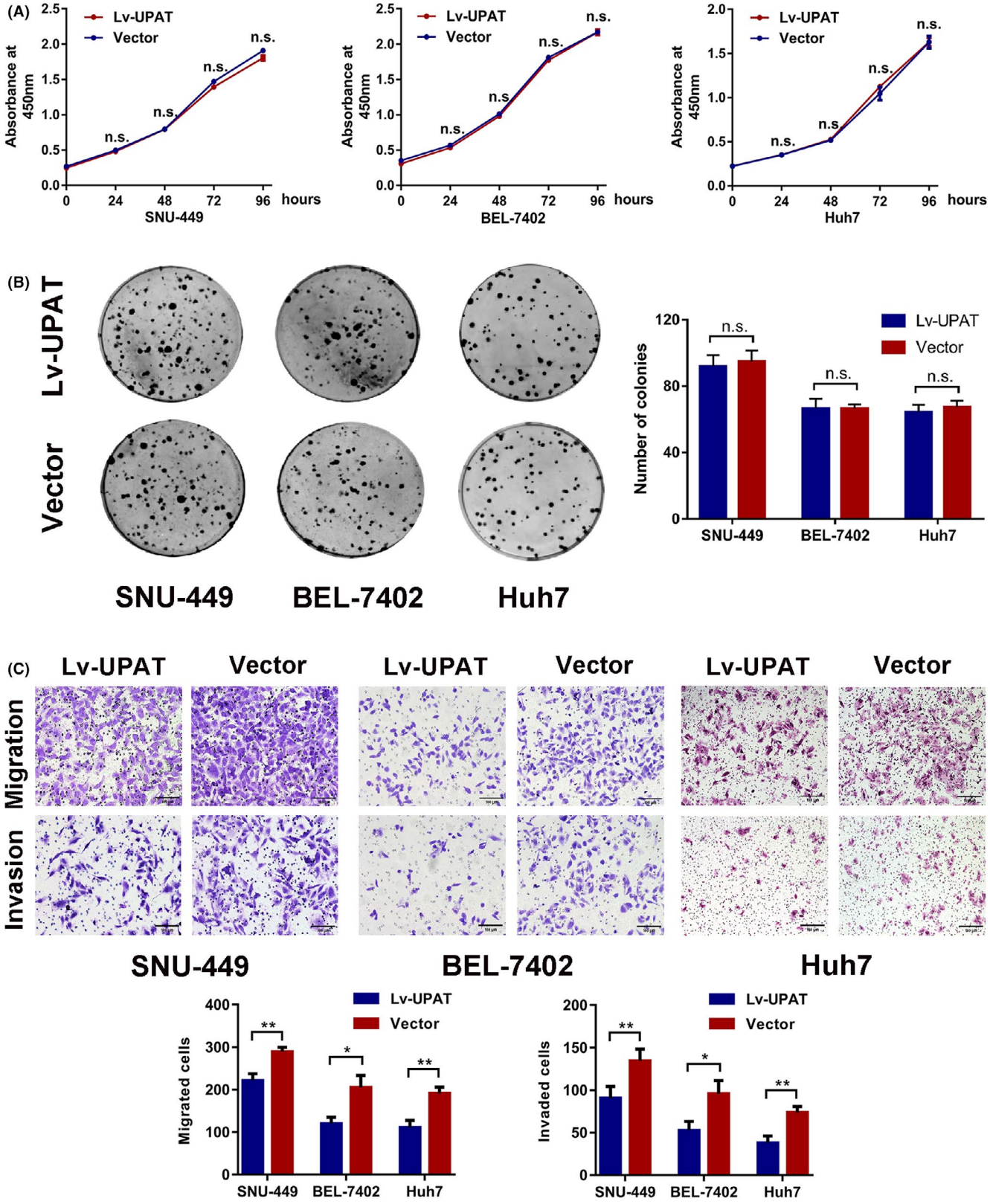

FIGURE 2 Effect of UHRF1 Protein Associated Transcript (UPAT) on cellular proliferation, migration, and invasion. A, Cellular proliferation was measured by CCK-8 assay in SNU-449, BEL-7402, and Huh7 cells after 0, 24,48, 72 and 96 h culture. B, Cellular proliferation was also evaluated by plate colony-forming assay in SNU-449, BEL-7402, and Huh7 cells after maintained for 14 d. C, Cell migratory and invasive abilities were measured in SNU-449, BEL-7402, and Huh7 cells by Transwell migration and invasion assays, respectively. Scale bars: 100 μm. n.s., not significant; $^{*}P < .05$; $^{**}P < .01$; $^{***}P < .001$

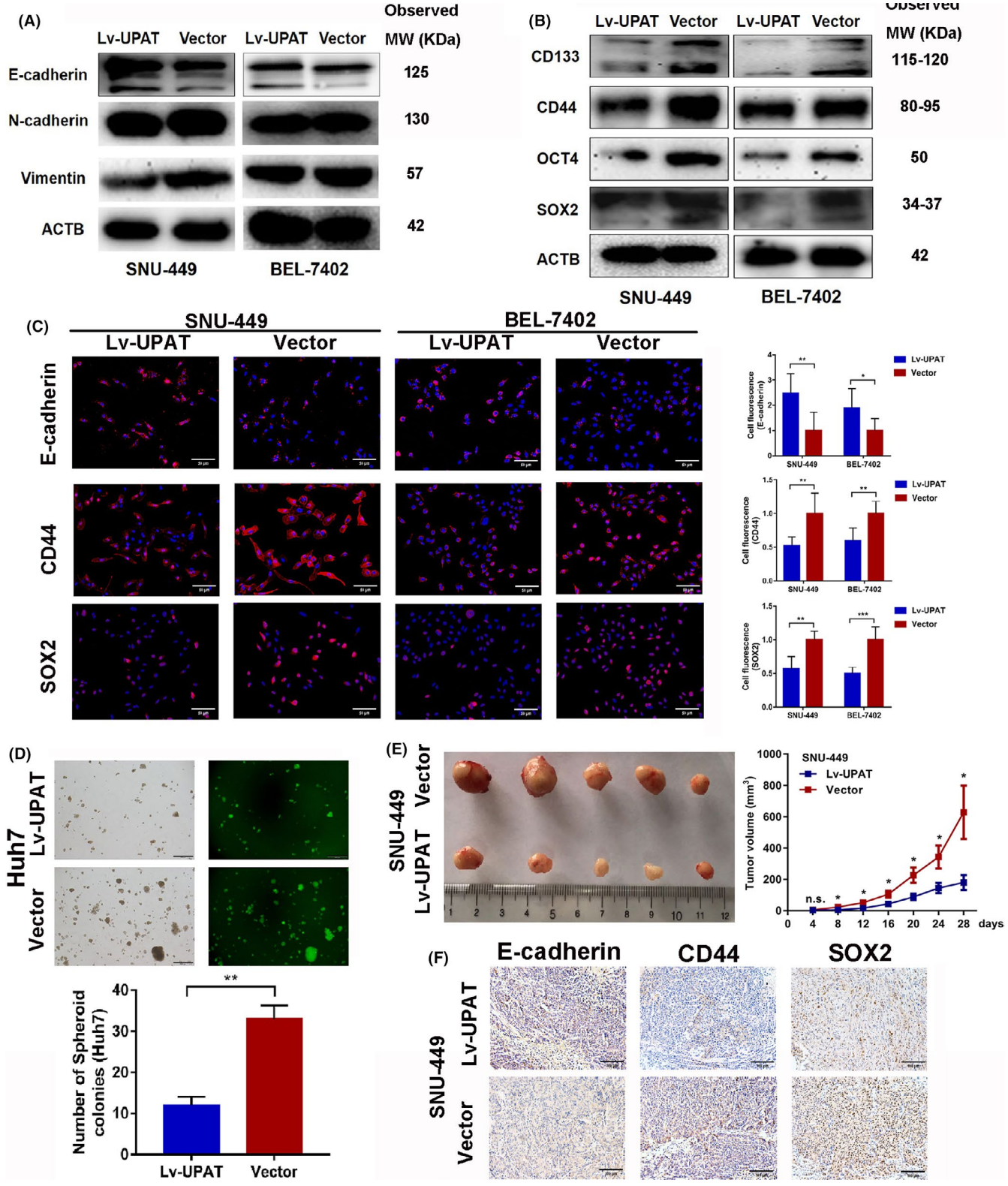

FIGURE 3 Effect of UHRF1 Protein Associated Transcript (UPAT) overexpression on epithelial-mesenchymal transition (EMT) and cancer stem cell (CSC) properties in HCC cell lines. A, B, Detection of EMT-related proteins (A, E-cadherin, N-cadherin and vimentin) and CSC-related proteins (B, CD133, CD44, OCT4, SOX2) using western blotting after forced expression of UPAT in SNU-449 and BEL-7402 cells. C, Representative images and comparisons of the E-cadherin, CD44, SOX2 expression by immunofluorescence staining in SNU-449 and BEL-7402 cells after UPAT overexpression. Scale bars: 50 μm). D, Evaluation of spheroid colonies formation ability after UPAT upregulation in Huh7 cells. Scale bars: 200 μm. E, UPAT-overexpressing or vector SNU-449 cells were subcutaneously injected into male BALB/c nude mice, the tumor volumes were measured every 4 d and harvested after 28 d. F, Expression of E-cadherin, CD44, and SOX2 were detected by immunohistochemistry in xenografts tissues. Scale bars: 100 μm. MW, molecular weight; $^{*}P < .05$; $^{**}P < .01$; $^{***}P < .001$

FIGURE 4 Effect and the molecular mechanism of UHRF1 Protein Associated Transcript (UPAT) on ZEB1 protein expression in HCC cell lines. A, Detection of ZEB1 mRNA in UPAT-upregulated SNU-449 and BEL-7402 cell lines by RT-qPCR. B-D, Detection of ZEB1 protein after UPAT overexpression in SNU-449 and BEL-7402 cell lines by immunofluorescence staining (B, C) and western blotting (WB) (D), UHRF1 protein was evaluated as positive control (D). Scale bars: 50 μm. E, Cells were treated with proteasome inhibitor, MG-132 (10 μM) for 24 h, and ZEB1 protein expression was determined by WB, UHRF1 protein were evaluated as positive control. F, To determine the degradation rate of ZEB1 protein, cells were treated with protein synthesis inhibitor, cycloheximide (10 μM) for 0, 1, 2, or 4 h, the ZEB1 protein expression were then determined by WB, the gray values of protein bands were evaluated using ImageJ software. G, Lv-UPAT and vector SNU-449 cells were treated with MG-132 (10 μM) for 24 h, then the protein lysates was immunoprecipitated with anti-ZEB1 monoclonal antibody and immunoblotted with ubiquitin (P4D1) for detection of ubiquitinated ZEB1. H, RNA immunoprecipitation assay was performed in SNU-449 lysates using anti-ZEB1 antibody and control IgG, the obtained RNA was subjected to RT-qPCR analysis to detect UPAT enrichment. MW, molecular weight; n.s., not significant; $^{*}P < .05$; $^{**}P < .01$; $^{***}P < .001$

3.2 | Overexpression of UPAT inhibits cellular migration and invasion in HCC cells

To understand the potential impact of UPAT on HCC progression, in vitro functional experiments were performed. Firstly, UPAT was found commonly downregulated in liver cancer cell lines as revealed by RT-qPCR assays (Figure S1A). Subcellular fractionation and RNAs quantification assays showed that UPAT was primarily located in the nucleus (Figure S1B). UPAT expressing sequence was synthesized and introduced into SNU-449, BEL-7402 and Huh7 cells using a lentivirus-based method (Figure S1C,D), and UPAT expression was dramatically increased in the Lv-UPAT groups compared with the vector groups (Figure S1C). Furthermore, FACS-based counting of GFP-expressing cells revealed that UPAT-containing or empty vectors were successfully transfected into liver cancer cell lines (Figure S1D). CCK-8 and plate colony formation assays indicated that cellular proliferation was not altered in SNU-449, BEL-7402, and Huh7 cell lines (Figure 2A,B), however migration and invasion were significantly suppressed in Lv-UPAT groups compared with the vector groups (Figure 2C). These results indicated that UPAT could function as a tumor suppressor in HCC progression.

3.3 | Overexpression of UPAT suppresses EMT and CSCs properties in HCC cells

To find the exact effect of UPAT in the development of HCC progression, bioinformatic analyses were conducted using UPAT co-expressed mRNAs obtained from cBioPortal.[26,27] To obtain useful results, mRNAs with their expression negatively correlated with UPAT were selected for further GO analyses using Database for Annotation, Visualization and Integrated Discovery (DAVID) after trying a variety of analysis methods (Figure S2A), and the top enriched clusters were presented.[28] As shown in Figure S2B, many mRNAs were enriched classified as cell-cell adhesion, MAPK cascade, proteasome-mediated ubiquitin-dependent protein catabolic process, negative regulation of canonical Wnt signaling pathway, and protein polyubiquitination (biological process), cell-cell adherens junction, proteasome complex, and proteasome core complex (cellular component). Cadherin binding was involved in cell-cell adhesion (molecular function), which indicated that UPAT could be close associated with HCC metastasis and the ubiquitin-proteasome associated pathway.

By undergoing the EMT program, tumor cells not only transfer to a mesenchymal phenotype, but also acquire CSC traits, resulting in metastatic recurrence of cancers.[8-10] Interestingly, the epithelial marker, E-cadherin was observed to be upregulated after overexpression of UPAT, while mesenchymal markers, N-cadherin and vimentin were decreased in SNU-449 and BEL-7402 cell lines (Figure 3A). At the same time, expression of CSC-associated markers, CD133 and CD44, as well as CSC-associated transcriptional factors, OCT4 and SOX2, were also found to be concurrently downregulated after overexpression of UPAT (Figure 3B). Changes in several key factors, E-cadherin, CD44 and SOX2 were validated again by IF staining (Figure 3C).

To evaluate the effect of UPAT on CSC traits of HCC cell lines, spheroid colony formation and tumor xenografts assays were conducted. Because of the inherent features of the SNU-449, BEL-7402 and Huh7 cell lines, only Huh7 was able to form spheroid colonies under the given conditions, and the results showed that overexpression of UPAT significantly inhibited spheroid colony formation (Figure 3D). Furthermore, Lv-UPAT or empty vector transfected SNU-449 cells were subcutaneously injected into BALB/c nude mice; UPAT-overexpressing tumors were observed to grow more slower than those of vector group (Figure 3E). In addition, the expression of some key factors, E-cadherin, CD44, and SOX2, was detected using IHC of xenograft tissues. E-cadherin levels were found to be significantly increased, while levels of CSC-related proteins, CD44 and SOX2 were decreased in UPAT-overexpressing xenograft tissues (Figure 3F).

3.4 | UPAT promotes ZEB1 degradation by ubiquitin-proteasome pathway

Our previous GO analyses indicated a close association of UPAT with ubiquitin-proteasome pathways (Figure S2B). Interestingly, UPAT was reported to promotes colon tumorigenesis by inhibiting the degradation of UHRF1 via interfering with β-TrCP1- and β-TrCP2-mediated ubiquitination. In addition, UPAT was thought to be an interesting ubiquitin-proteasome system associated pseudogene because of its binding to multiple ubiquitin-proteasome system associated proteins, such as cullin9, PSMD2, UIMC1, and UHRF1. Also, ZEB1, a key EMT and CSC driver,[18] also binds to UPAT.[14] Therefore, to define the mechanism for UPAT suppression of EMT and CSCs

properties in HCC, we evaluated the interaction between ZEB1 and UPAT from the perspective of the ubiquitin-proteasome pathway.

Initially, the baseline expression of ZEB1 protein was evaluated in a subset of liver cancer cell lines (Figure S3). After UPAT overexpression, ZEB1 was found to have decreased protein levels, rather than mRNA levels (Figure 4A-D), while UHRF1 expression was also evaluated as a positive control (Figure 4D). When treated with proteasome inhibitor, MG-132, for 24 h, the expression of ZEB1

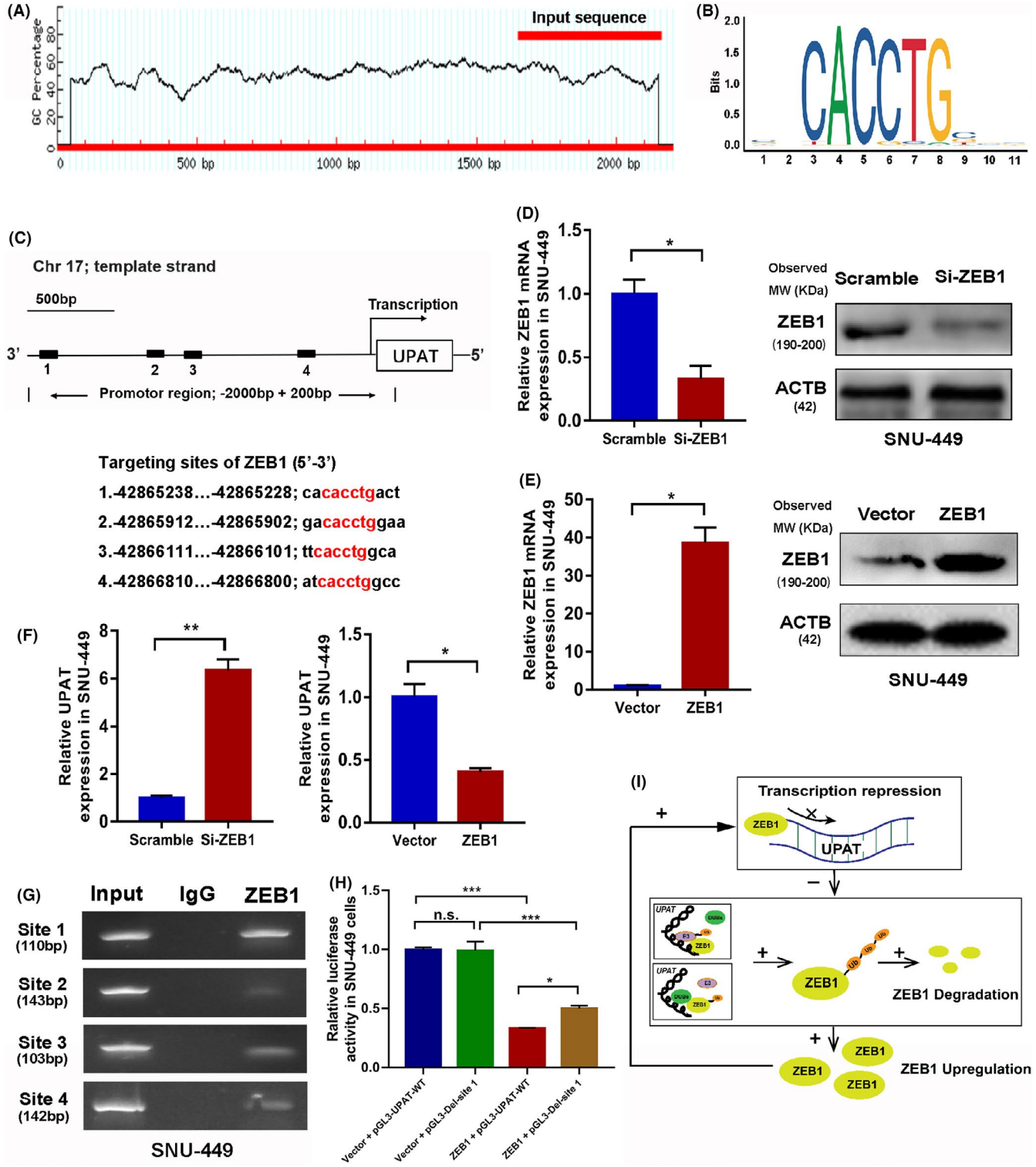

protein was dramatically restored (Figure 4E). Moreover, the turnover rate of ZEB1 protein was decreased from approximately 2 h to less that 1 h in Lv-UPAT cells after whole protein synthesis was blocked with cycloheximide (Figure 4F). Furthermore, a ubiquitination assay revealed that ZEB1 ubiquitination levels were significantly upregulated after UPAT overexpression, and treatment with MG-132 significantly amplified this difference (Figure 4G). Additionally, RIP assay showed that the anti-ZEB1 antibody significantly enriched UPAT compared with a non-specific IgG control (Figure 4H). These results suggested that UPAT directly or indirectly binds to ZEB1 and promotes ZEB1 degradation through a ubiquitin-proteasome pathway.

FIGURE 5 ZEB1 transcriptionally suppresses UHRF1 Protein Associated Transcript (UPAT) expression in hepatocellular carcinoma (HCC) cell line and the brief elucidation of their interaction. A, CpG island prediction in the promoter region of UPAT using MethPrimer. B, ZEB1 specifically binding element, the E-box-like element (CACCTG). C, Four E-box-like elements were found in the promoter region of UPAT in the template strand. D, ZEB1 was knocked down using targeted siRNA in SNU-449 cells, its mRNA (left) and protein (right) levels were determined by RT-qPCR and western blotting (WB), respectively. E, ZEB1 was transiently upregulated using plasmid in SNU-449 cells, its mRNA (left) and protein (right) levels were determined by RT-qPCR and WB, respectively. F, UPAT expression was evaluated by RT-qPCR after successfully ZEB1 knockdown (left) or upregulation (right) in SNU-449 cells. G, Chromatin immunoprecipitation (ChIP)-PCR assay was conducted to evaluate the binding of ZEB1 to the predicted targeting sites. H, Dual-luciferase reporter assay was performed to evaluate the transcriptional regulation of ZEB1 on the predicted promoter region and binding site 1 deleted promoter region of UPAT. I, Brief elucidation of ZEB1-UPAT positive feedback loop. Upregulated ZEB1 in HCC transcriptionally represses UPAT expression, UPAT deficiency impairs the ubiquitin-proteasome pathway associated ZEB1 degradation, thereby results in ZEB1 overexpression and reinforcement of the above track. MW, molecular weight; WT, wild-type; Del-site 1, binding site 1 deleted; n.s., not significant; $^{*}P < .05$; $^{**}P < .01$; $^{***}P < .001$

3.5 | ZEB1 transcriptionally suppresses UPAT expression in HCC cell line

The mechanism that results in UPAT deficiency in cancers is still unknown. We speculated that dysfunction of transcriptional regulation may be part of the reason. To address this issue, the promoter region of UPAT was obtained using UCSC online software.[24] The CpG island was predicted using MethPrimer to preliminarily evaluate whether DNA methylation in the promoter region of UPAT controls its transcription.[29] The results showed that no CpG island exists in the promoter region of UPAT (Figure 5A). However, JASPAR revealed that hundreds of TFs bound to the promoter region and could regulate UPAT transcription. Of them, the 4 most probably binding motifs (score > 10) for ZEB1 were found to lie within the predicted promoter region of the template strand (Figure 5B,C).[25] It is well known that ZEB1 usually binds to E-box-like promoter elements (5′-CACCTG-3′) of the target gene through its C2H2-type zinc finger clusters. Thereafter it activates or obstructs transcription by recruiting co-activators or co-suppressors through the SMAD interaction domain (SID), CtBP interaction domain (CID), and p300-P/CAF binding domain (CBD).[18] To evaluate whether ZEB1 inversely inhibits UPAT expression, ZEB1 was transiently knocked down or forced to be expressed by specific siRNA or plasmid in SNU-449 cell line (Figure 5D,E), and UPAT levels were found to be significantly upregulated or downregulated, respectively (Figure 5F). Moreover, ChIP-PCR experiments showed the significant enrichment of ZEB1 in these 4 predicted binding sites compared with control IgG, especially in site 1 (Figure 5G). In addition, the predicted promoter region (pGL3-UPAT-WT) or binding site 1-deleted promoter region (pGL3-Del-site 1) of UPAT was cloned into the pGL3-Basic plasmid, and the transcriptional regulation of ZEB1 was investigated through a dual-luciferase reporter assay. SNU-449 cells were co-transfected with ZEB1 overexpression or vector plasmids and pGL3-UPAT-WT or pGL3-Del-site 1 plasmids. As shown in Figure 5H, pGL3-UPAT-WT and pGL3-Del-site 1 promoter activities were both notably inhibited by ZEB1. However, the inhibition efficiency of ZEB1 for the pGL3-Del-site 1 was significantly weaker than that of pGL3-UPAT-WT. These results together indicated that ZEB1 reversely suppressed UPAT expression at the transcriptional level, and could be partly the way that it contributes to UPAT deficiency in HCC.

3.6 | The negative correlation between UPAT and ZEB1 and their significance in HCC tissues

Following the investigation of the UPAT interplay with ZEB1 in HCC cell lines (Figure 5H), correlation between UPAT and ZEB1 in clinical tissues was then evaluated. ZEB1 protein expression was determined by IHC in HCC and adjacent noncancerous tissues of 54 patients who had been randomly selected from the previous cohort. As shown in Figure 6A,B, ZEB1 was primarily located in the nucleus and upregulated in HCC tissues compared with adjacent noncancerous tissues. The positive rate of ZEB1 protein in HCC tissues (48.15%, 26/54) was significantly higher than that in adjacent benign tissues (5.56%, 3/54; Figure 6C). Patients with lower relative UPAT expression in HCC tissues were inclined to have higher ZEB1 protein levels (Figure 6D). Furthermore, Pearson correlation analysis indicated a significant negative correlation between ZEB1 protein and relative UPAT expressions (correlation coefficient $r = -0.354$, $P = .0086$, n = 54; Figure 6E). In addition, patients were divided into 2 groups based on the median value (median = 2.603) of relative UPAT expression (< median, lower UPAT group, n = 27; >median, higher UPAT group, n = 27) or ZEB1 protein expression (score 0, lower group, n = 28; ≥1, higher group, n = 26), respectively, and into 4 groups based on combined UPAT and ZEB1 protein expression (Figure 6E). Kaplan-Meier analysis together with UPAT or ZEB1 expression showed that patients with higher UPAT values (lower group, median RFS, 312 d vs higher group, median RFS undefined) and lower ZEB1 values (lower group, median RFS undefined vs higher group, median RFS 359.5 d) had better RFS, even though no significance between lower/higher ZEB1 groups was observed; furthermore, patients in the $UPAT_{higher}$ $ZEB1_{lower}$ and $UPAT_{higher}$ $ZEB1_{higher}$ groups had prolonged RFS (median, Undefined). Patients in the $UPAT_{lower}$ $ZEB1_{lower}$ group had a moderate RFS (median, 422 d), while patients with lower UPAT and higher ZEB1 protein expression had the worst prognosis (median, 187.5 d; $P = .0073$; Figure 6F).

4 | DISCUSSION

Increasing studies have uncovered the functions and significance of pseudogenes in tumorigenesis and progression of cancers, however only a few studies focused on pseudogene associated HCC metastasis.

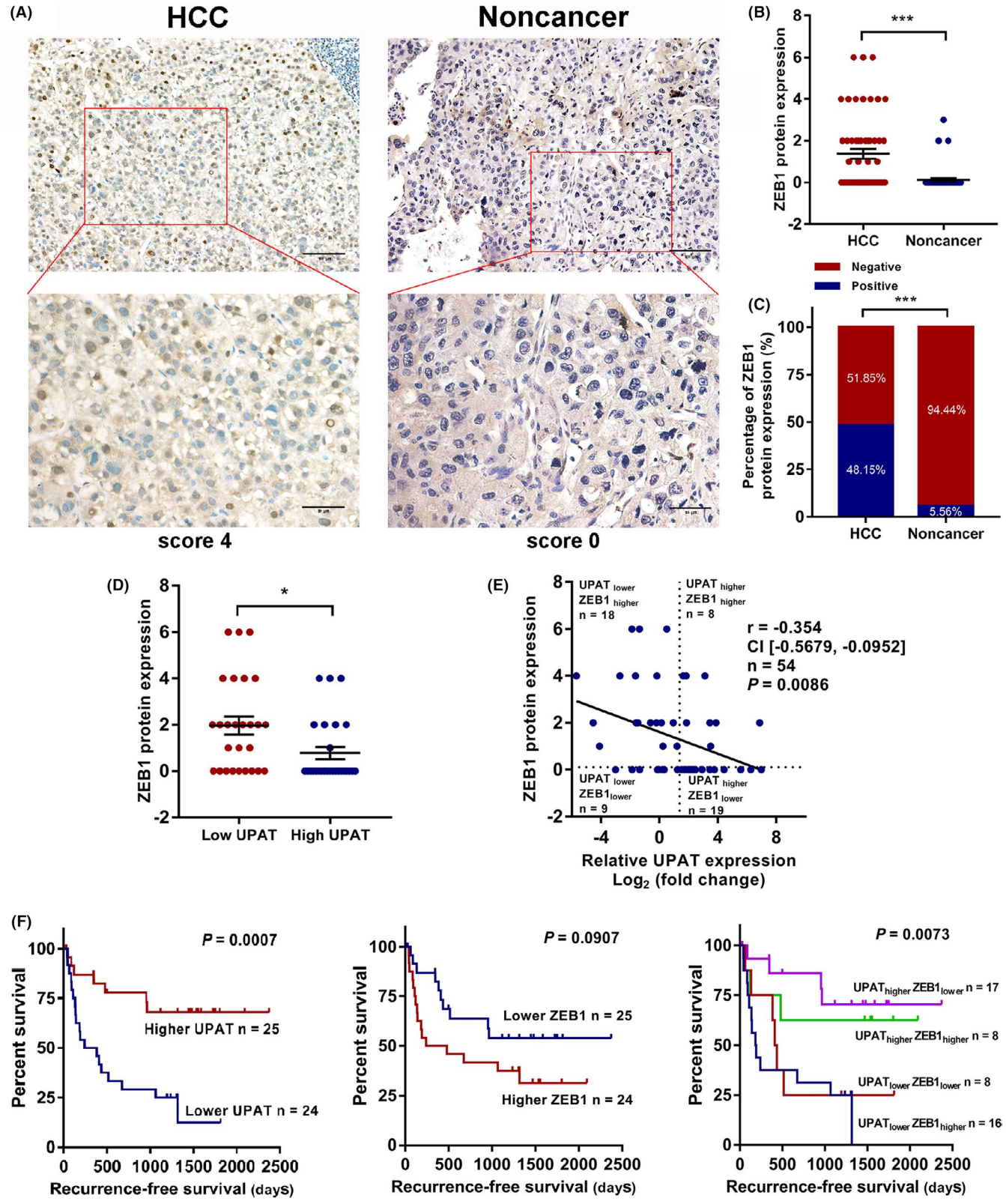

Here, we investigated a tumor suppressor pseudogene, UPAT, that was transcriptionally suppressed by ZEB1 in HBV-related HCC. Accordingly, UPAT deficiency impaired ubiquitin-proteasome pathway-related ZEB1 degradation. By forming this UPAT/ZEB1 positive feedback loop, HCC cells were able to maintain EMT and CSC properties.

UPAT expression used to be thought not relevant for hepatic virus infection, including HBV and HCV. In a previous study, Wang et al[17] determined UPAT expression in 108 patients with HCC, including 5 patients without HBV infection and 3 patients without HCV infection. They indicated that at least 92.59% (100/108) of

FIGURE 6 Negative correlation between UHRF1 Protein Associated Transcript (UPAT) and ZEB1 protein in hepatocellular carcinoma (HCC) tissues and their clinical significance in post–operative survival. A, Representative images of ZEB1 protein expression determined by IHC staining in HCC tissues. Scale bars, upper row, 100 μm; lower row, 50 μm). B, ZEB1 protein expression was compared between HCC and adjacent noncancerous liver tissues using *t* test (n = 54). C, Positive rate of ZEB1 protein was compared between HCC and adjacent noncancerous liver tissues using chi-square test. D, ZEB1 protein expression was compared between HCC patients grouped with relative UPAT expression using *t* test. E, Pearson correlation analysis between UPAT and ZEB1 protein expression in patients with HCC ($r = -0.354$, n = 54, $P = 0.0086$), the broken lines indicate the median of relative UPAT expression (median = 2.603) and the cutoff score of ZEB1 protein. F, Kaplan-Meier analysis of recurrence-free survival (RFS) in patients with UPAT higher (> median)/lower (< median), ZEB1 higher (score ≥ 1)/lower (score = 0), and combined UPAT and ZEB1 protein expression, 3 patients were loss to follow-up and 2 were removed from prognostic analysis because of post–operative complication-related death. $^{*}P < .05$; $^{**}P < .01$; $^{***}P < .001$

the recruited patients were diagnosed with HBV and HCV co-infection-related HCC, and the results suggested that UPAT was decreased in 68% of HCC tissue samples. Its expression was negatively correlated with advanced clinical stage, capsule invasion, and vessel invasion, but was not relevant to HBV and HCV infection. However, the occurrence of HBV-related HCC is always observed in non-cirrhotic livers,[30] and the occurrence and post–operative recurrence of HCC significantly increases with the HBV-DNA load.[31,32] In-depth studies revealed that following HBV integration into the human genome, wild-type and mutated viral proteins, and HBV genetic variability independently contribute to the development of HCC.[30] These discoveries together indicated that HBV exerts unique influences on tumorigenesis and progression of HCC, and ensuring the homogeneity of the recruited patients is crucial while elucidating the clinical significance of UPAT expression. In this study, when determining UPAT expression in a cohort of HBV-related HCC, approximately 40% of patients showed low relative UPAT expression in cancerous tissues, and its expression significantly decreased with increase in HBV-DNA copies, which as quite different from previous reports. Potential mechanisms could exist for HBV involved UPAT deficiency other than ZEB1 induced transcriptional repression, and this needs further elucidation.

The exact roles of UPAT in the EMT process is divergent in cancer types.[15-17] Based on bioinformatics analysis and the correlation between UPAT expression and MVI, we preliminarily discovered that UPAT not only inhibits the EMT process, but also controls the acquisition of CSC properties by suppressing the expression of CSC-related TFs and markers. It limits the formation of spheroid colonies and tumor xenografts; limiting dilution assays, including a wide range of serial dilutions for in vivo tumor xenografts assay and in vitro sphere-forming assay, would be helpful to further support this observation. The mechanistic studies revealed that ZEB1, a well known EMT and CSC-related TF, was notably downregulated after UPAT overexpression. In addition, the promotion of ZEB1 ubiquitination and reduction of ZEB1 protein half-life after UPAT overexpression were observed, as well as the binding between UPAT and ZEB1 protein. Furthermore, UPAT was negatively correlated with ZEB1 protein level in HBV-related HCC tissues. These results strongly propose that UPAT limits the EMT and CSCs properties of HCC by promoting ZEB1 degradation. However, a recent study reported the opposite effects of UPAT on EMT and ZEB1 protein expression in gastrointestinal stromal tumor cell, but unfortunately, mechanistic experiments were not carried out.[15] We speculate that the interaction of UPAT and ZEB1 may explain this contradiction.

EMT-TFs are short-lived proteins that are rapidly regulated by the ubiquitin-proteasome system through specific E3 ubiquitin ligases and deubiquitinating enzymes (DUBs), which keeps EMT-TFs at low levels in normal tissues.[33] Limited research has addressed the ubiquitin-proteasome system controlled ZEB1 protein degradation. To date, SIAH1/2 and FBXO45 are thought to be the only 2 ubiquitin E3 ligases promoting ZEB1 ubiquitination; FLASH protects ZEB1 from proteosomal degradation by interplay with SIAH1 and FBXO45.[34-36] Zhou et al[37] also proposed that 4 ubiquitin-specific proteases (USPs), including USP7, USP10, USP29, and particularly USP51, could be responsible for deubiquitinating ZEB1. As a potential ubiquitination-associated pseudogene, UPAT directly binds to multiple ubiquitin E3 ligases, such as cullin9, PSMD2, UIMC1, and UHRF1.[14] However, none of these proteins was reported to regulate ZEB1 ubiquitination. We speculate that UPAT could either directly recruit unknown ubiquitin E3 ligases to ZEB1 protein or interfere with ZEB1 de-ubiquitination by inhibiting the ubiquitin protease activity of potential DUBs. This area requires further study.

In conclusion, we found that the pseudogene UPAT promotes the degradation of ZEB1 through the ubiquitin-proteasome pathway, and in contrast, the expression of UPAT is transcriptionally restrained by ZEB1. Dysregulation of the UPAT-ZEB1 circuit may play a key role in the progression of EMT and CSC traits of HCC. Illustrating the potential mechanism may help the development of novel therapies to prevent HCC metastasis.

ACKNOWLEDGMENTS

This work was supported by the Guangdong Provincial Science and Technology Projects (grant number, 2017A020215132) and the National Natural Science Foundation of China (grant number, 81872385). The authors thank Professor Weizhong Wu, Liver Cancer Research Institute, Zhongshan Hospital, Fudan University, Shanghai, China, for providing the HCC cell lines MHCC-LM3, MHCC-97H, and MHCC-97L as a gift, and Editage for English language editing services.

CONFLICT OF INTEREST

None.

ORCID

Dinghua Yang https://orcid.org/0000-0002-1442-5240

REFERENCES

1. Forner A, Reig M, Bruix J. Hepatocellular carcinoma. *Lancet*. 2018;391:1301-1314.
2. Bray F, Ferlay J, Soerjomataram I, Siegel RL, Torre LA, Jemal A. Global cancer statistics 2018: GLOBOCAN estimates of incidence and mortality worldwide for 36 cancers in 185 countries. *CA Cancer J Clin*. 2018;68:394-424.
3. Sherman M. Hepatocellular carcinoma: epidemiology, surveillance, and diagnosis. *Semin Liver Dis*. 2010;30:3-16.
4. Wang M, Wang Y, Feng X, et al. Contribution of hepatitis B virus and hepatitis C virus to liver cancer in China north areas: Experience of the Chinese National Cancer Center. *Int J Infect Dis*. 2017;65:15-21.
5. Hasegawa K, Kokudo N, Makuuchi M, et al. Comparison of resection and ablation for hepatocellular carcinoma: a cohort study based on a Japanese nationwide survey. *J Hepatol*. 2013;58:724-729.
6. Nieto MA, Huang RY, Jackson RA, Thiery JP. Emt: 2016. *Cell*. 2016;166:21-45.
7. Shibue T, Weinberg RA. EMT, CSCs, and drug resistance: the mechanistic link and clinical implications. *Nat Rev Clin Oncol*. 2017;14:611-629.
8. Kusoglu A, Biray AC. Cancer stem cells: A brief review of the current status. *J Cell Physiol*. 2019;681:80-85.
9. Puisieux A, Brabletz T, Caramel J. Oncogenic roles of EMT-inducing transcription factors. *Nat Cell Biol*. 2014;16:488-494.
10. Singh M, Yelle N, Venugopal C, Singh SK. EMT: mechanisms and therapeutic implications. *Pharmacol Ther*. 2018;182:80-94.
11. Scheel C, Eaton EN, Li SH, et al. Paracrine and autocrine signals induce and maintain mesenchymal and stem cell states in the breast. *Cell*. 2011;145:926-940.
12. Taube JH, Herschkowitz JI, Komurov K, et al. Core epithelial-to-mesenchymal transition interactome gene-expression signature is associated with claudin-low and metaplastic breast cancer subtypes. *Proc Natl Acad Sci USA*. 2010;107:15449-15454.
13. Schwelberger HG. The origin of mammalian plasma amine oxidases. *J Neural Transm*. 2007;114:757-762.
14. Taniue K, Kurimoto A, Sugimasa H, et al. Long noncoding RNA UPAT promotes colon tumorigenesis by inhibiting degradation of UHRF1. *Proc Natl Acad Sci USA*. 2016;113:1273-1278.
15. Hu JC, Wang Q, Jiang LX, et al. Effect of long non-coding RNA AOC4P on gastrointestinal stromal tumor cells. *Onco Targets Ther*. 2018;11:6259-6269.
16. Zhang K, Lu C, Huang X, et al. Long noncoding RNA AOC4P regulates tumor cell proliferation and invasion by epithelial-mesenchymal transition in gastric cancer. *Ther Adv Gastroenterol*. 2019;12:1756284819827697.
17. Wang TH, Lin YS, Chen Y, et al. Long non-coding RNA AOC4P suppresses hepatocellular carcinoma metastasis by enhancing vimentin degradation and inhibiting epithelial-mesenchymal transition. *Oncotarget*. 2015;6:23342-23357.
18. Caramel J, Ligier M, Puisieux A. Pleiotropic roles for ZEB1 in cancer. *Cancer Res*. 2018;78:30-35.
19. Wellner U, Schubert J, Burk UC, et al. The EMT-activator ZEB1 promotes tumorigenicity by repressing stemness-inhibiting microRNAs. *Nat Cell Biol*. 2009;11:1487-1495.
20. Shimono Y, Zabala M, Cho RW, et al. Downregulation of miRNA-200c links breast cancer stem cells with normal stem cells. *Cell*. 2009;138:592-603.
21. Chaffer CL, Marjanovic ND, Lee T, et al. Poised chromatin at the ZEB1 promoter enables breast cancer cell plasticity and enhances tumorigenicity. *Cell*. 2013;154:61-74.
22. Mladinich M, Ruan D, Chan CH. Tackling cancer stem cells via inhibition of EMT transcription factors. *Stem Cells Int*. 2016;2016:5285892.
23. Xiang LY, Ou HH, Liu XC, et al. Loss of tumor suppressor miR-126 contributes to the development of hepatitis B virus-related hepatocellular carcinoma metastasis through the upregulation of ADAM9. *Tumour Biol*. 2017;39:1010428317709128.
24. Kent WJ, Sugnet CW, Furey TS, et al. The human genome browser at UCSC. *Genome Res*. 2002;12:996-1006.
25. Khan A, Fornes O, Stigliani A, et al. JASPAR 2018: update of the open-access database of transcription factor binding profiles and its web framework. *Nucleic Acids Res*. 2018;46:D1284.
26. Gao J, Aksoy BA, Dogrusoz U, et al. Integrative analysis of complex cancer genomics and clinical profiles using the cBioPortal. *Sci Signal*. 2013;6:pl1.
27. Cerami E, Gao J, Dogrusoz U, et al. The cBio cancer genomics portal: an open platform for exploring multidimensional cancer genomics data. *Cancer Discov*. 2012;2:401-404.
28. da Huang W, Sherman BT, Lempicki RA. Systematic and integrative analysis of large gene lists using DAVID bioinformatics resources. *Nat Protoc*. 2009;4:44-57.
29. Li LC, Dahiya R. MethPrimer: designing primers for methylation PCRs. *Bioinformatics*. 2002;18:1427-1431.
30. Levrero M, Zucman-Rossi J. Mechanisms of HBV-induced hepatocellular carcinoma. *J Hepatol*. 2016;64:S84-s101.
31. Chen CJ, Yang HI, Su J, et al. Risk of hepatocellular carcinoma across a biological gradient of serum hepatitis B virus DNA level. *JAMA*. 2006;295:65-73.
32. Meng C, Liu T, Liu YW, Zhang LZ, Wang YL. Hepatitis B virus cccDNA in hepatocellular carcinoma tissue increases the risk of recurrence after liver transplantation. *Transplant Proc*. 2019;51:3364-3368.
33. Diaz VM, de Herreros AG. F-box proteins: keeping the epithelial-to-mesenchymal transition (EMT) in check. *Semin Cancer Biol*. 2016;36:71-79.
34. Chen A, Wong CSF, Liu MCP, et al. The ubiquitin ligase Siah is a novel regulator of Zeb1 in breast cancer. *Oncotarget*. 2015;6:862-873.
35. Xu M, Zhu C, Zhao X, et al. Atypical ubiquitin E3 ligase complex Skp1-Pam-Fbxo45 controls the core epithelial-to-mesenchymal transition-inducing transcription factors. *Oncotarget*. 2015;6:979-994.
36. Abshire CF, Carroll JL, Dragoi AM. FLASH protects ZEB1 from degradation and supports cancer cells' epithelial-to-mesenchymal transition. *Oncogenesis*. 2016;5:e254.
37. Zhou Z, Zhang P, Hu X, et al. USP51 promotes deubiquitination and stabilization of ZEB1. *Am J Cancer Res*. 2017;7:2020-2031.

SUPPORTING INFORMATION

Additional supporting information may be found online in the Supporting Information section.

How to cite this article: Xiang L, Huang X, Wang S, et al. Deficiency of pseudogene UPAT leads to hepatocellular carcinoma progression and forms a positive feedback loop with ZEB1. *Cancer Sci*. 2020;111:4102–4117. https://doi.org/10.1111/cas.14620